Mitochondrial Retrograde Signaling Mediated by UCP2 Inhibits Cancer Cell Proliferation and Tumorigenesis

P. Esteves, C. Pecqueur, C. Ransy, C. Esnous, V. Lenoir, F. Bouillaud, A.-L. Bulteau, A. Lombes, C. Prip-Buus, D. Ricquier, et al.

Tumor and Stem Cell Biology

Cancer Research

Mitochondrial Retrograde Signaling Mediated by UCP2 Inhibits Cancer Cell Proliferation and Tumorigenesis

Pauline Esteves[1,2,3], Claire Pecqueur[4,5], Céline Ransy[1,2,3], Catherine Esnous[1,2,3], Véronique Lenoir[1,2,3], Frédéric Bouillaud[1,2,3], Anne-Laure Bulteau[1,2,3], Anne Lombès[1,2,3], Carina Prip-Buus[1,2,3], Daniel Ricquier[1,2,3], and Marie-Clotilde Alves-Guerra[1,2,3]

Abstract

Cancer cells tilt their energy production away from oxidative phosphorylation (OXPHOS) toward glycolysis during malignant progression, even when aerobic metabolism is available. Reversing this phenomenon, known as the Warburg effect, may offer a generalized anticancer strategy. In this study, we show that overexpression of the mitochondrial membrane transport protein UCP2 in cancer cells is sufficient to restore a balance toward oxidative phosphorylation and to repress malignant phenotypes. Altered expression of glycolytic and oxidative enzymes mediated the effects of this metabolic shift. Notably, UCP2 overexpression increased signaling from the master energy-regulating kinase, adenosine monophosphate-activated protein kinase, while downregulating expression of hypoxia-induced factor. In support of recent new evidence about UCP2 function, we found that UCP2 did not function in this setting as a membrane potential uncoupling protein, but instead acted to control routing of mitochondria substrates. Taken together, our results define a strategy to reorient mitochondrial function in cancer cells toward OXPHOS that restricts their malignant phenotype. *Cancer Res; 74(14); 3971–82. ©2014 AACR.*

Introduction

Cancer is a multistep process involving gene modifications and chromosomal rearrangements in the tumor cells that promote unchecked proliferation, abrogate cell death, and reprogram metabolism (1, 2). Indeed, tumor cell proliferation requires rapid synthesis of macromolecules, including lipids, proteins, and nucleotides. Dysregulation of cellular metabolism has been associated with malignant transformation and may be triggered directly through mutations in oncogenes or through signaling pathways involved in metabolism (2, 3). Many cancer cells exhibit rapid glucose consumption, with most of the glucose-derived carbon being secreted as lactate despite abundant oxygen availability (Warburg effect). Glycolysis is also important for generating precursors and reducing equivalents needed for cellular biogenesis and antioxidant defense (4). Moreover, the bioenergetic reprogramming of tumoral cells from oxidative phosphorylation (OXPHOS) to the use of glycolysis for ATP production allows cells to be metabolically less oxygen dependent, thus favoring invasion processes.

Mitochondria have been directly involved in tumor development (5). Indeed, cancer-associated mutations have been identified in several metabolic enzymes genes such as the ones coding succinate dehydrogenase (SDH), fumarate hydratase (FH), and isocitrate dehydrogenase (IDH), all enzymes of the tricarboxylic acid cycle (TCA; refs. 6–8). In addition, in tight relation to their bioenergetic status, mitochondria play a crucial role in the control of apoptosis, are known to release reactive oxygen species (ROS), and contain potent antioxidant defense. Acting on metabolism, and more particularly on mitochondria, thus represents a therapeutic perspective for cancer therapy (9).

The uncoupling protein 2 (UCP2) is the second member identified in the UCP family (10), a subfamily of the mitochondrial carriers. The first member, UCP1, acts as a passive proton transporter in the mitochondrial inner membrane in brown adipose tissue (BAT). In this tissue, upon cold exposure, the mitochondrial respiration is uncoupled, meaning that the electron transport chain is no longer coupled to ATP synthesis. UCP2 exhibits singular features that distinguish it from the other uncoupling proteins. UCP2 mRNA is found in many tissues, whereas UCP1 and UCP3 are respectively restricted to BAT and muscle. UCP2 is regulated at both the transcriptional and translational levels (11, 12). The inhibition of UCP2 translation can be relieved *in vitro* by addition of glutamine and *in vivo* by fasting or an inflammatory state. Furthermore, the half-life of the protein is very short (13), suggesting that UCP2 is a suitable candidate for regulating rapid biologic responses. At

Authors' Affiliations: [1]Inserm, U1016, Institut Cochin; [2]CNRS, UMR 8104; [3]Université Paris Descartes, Sorbonne Paris Cité, Paris; [4]CRCNA—UMR 892 INSERM—6299 CNRS; and [5]Faculté de Médecine, Université de Nantes, Nantes, France

Note: Supplementary data for this article are available at Cancer Research Online (http://cancerres.aacrjournals.org/).

Current address for A.-L. Bulteau: LCABIE—CNRS UMR 5254—Université de Pau, Pau 64053, France.

Corresponding Author: Marie-Clotilde Alves-Guerra, Inserm U1016 Institut Cochin, Département Endocrinologie, Métabolisme et Diabète, Faculté de médecine, 24 rue du Faubourg Saint-Jacques, 75014 Paris, France. Phone: 331-5373-2706; Fax: 331-5373-2757; E-mail: clotilde.alves-guerra@inserm.fr

doi: 10.1158/0008-5472.CAN-13-3383

first, sequence similarities between UCP proteins led to the conclusion that they act in a similar way but with different intensities due to the lower UCP2 and UCP3 expression level compared with UCP1 (11). The generation of *Ucp2*$^{-/-}$ mice allowed us to show that UCP2 mitigates immunity through a reduction in ROS production (11, 14) and plays a role in inflammation (11, 15–17). Although partial uncoupling would decrease mitochondrial ROS release, our present point of view is that activities other than uncoupling have to be considered for UCP2. Previously, we showed that loss of UCP2 is associated with increased proliferation in primary fibroblasts (18). Interestingly, although no difference in the mitochondrial respiration and the ATP/ADP ratio was recorded, we demonstrated that *Ucp2*$^{-/-}$ fibroblasts were more dependent on glucose and oxidized less long-chain fatty acids. The correlation between higher rate of division and increased dependency to glucose in the absence of UCP2 recalls the Warburg hypothesis on metabolic alteration in cancer. Its present reformulation takes into account that complete oxidation leads to the loss of carbon skeleton. Consequently, dividing cells with an intense biosynthesis rate depend on a shift toward a larger availability of precursors favoring aerobic glycolysis. Therefore, UCP2 is a good candidate to understand the crosstalk between metabolic alteration and promotion of cancer initiation, progression, and invasion.

Our goal was to determine whether UCP2 is able to control metabolic reprogramming in cancer cells and to modify their proliferation. In this article, we show that cells overexpressing UCP2 shift their metabolism from glycolysis toward oxidative phosphorylation and become poorly tumorigenic. UCP2 overexpression generates a mitochondrial retrograde signaling that modifies expression of glycolytic and oxidative enzymes, leading to enhanced oxidative phosphorylation. Moreover, UCP2 overexpression is associated with an activation of adenosine monophosphate-activated protein kinase (AMPK) signaling together with a downregulation of hypoxia-induced factor (HIF) expression. Finally, UCP2 overexpression can amplify apoptosis induced by chemotherapeutic drugs, such as staurosporine. The crucial role of UCP2 in tumor metabolism makes UCP2 a promising target for tumor therapy.

Materials and Methods

Generation of UCP2-overexpressing cells

B16F10, MIA PaCa-2, and U-87 MG cells were obtained from ATCC. cDNA encoding the complete coding region of mouse *Ucp2* was subcloned into pcDNA vector, which contains a FLAG tag and neomycin resistance and then transfected in cells using lipofectamine 2000 (Invitrogen). Stable cell lines were selected following G418 treatment (0.5 mg/mL).

Colony-formation assay

Cells plated at low density (100 cells/well) in 6-well plate were cultured in their medium complemented or not, with 5 or 10 mmol/L dichloroacetate (DCA; Sigma), or with 100, 250 or 500 μmol/L 5-amino-1-β-D-ribofuranosyl-imidazole-4-carboxamide (AICAR; Toronto Research) or with 5 or 10 nmol/L Mito-TEMPO (Enzo). After 10 days of culture, colonies were stained with 0.05% (w/v) crystal violet in 80% (v/v) ethanol for 2 hours, and the corresponding optical density (OD) was read at 570 nm.

Western blot analysis

Cellular lysis was performed using a lysis buffer (1.5 mmol/L EDTA, 50 mmol/L Hepes pH7.4, 150 mmol/L NaCl, 10% (v/v) glycerol, and 1% (v/v) NP40). Mitochondrial fractions were isolated as described previously (11). Total cellular lysates and mitochondrial fractions were loaded onto a 4% to 20% SDS-PAGE gel (Bio-Rad), transferred onto nitrocellulose membrane, and revealed with different antibodies as homemade anti-UCP2 (UCP2–606; ref. 11) and homemade anti-HNE 4-hydroxy-nonenal (19). Commercial antibodies are listed in Supplementary Materials and Methods. Direct recording of the chemiluminescence (GeneGnome Syngene) and quantification (GeneSnap software) were performed (Ozyme). Western blot analyses were done using independent samples from independent cultures.

Oxygen consumption

Cells in their medium were introduced in the respiratory chamber of an oxygraph O2 k (Oroboros). Cellular respiration was determined under basal conditions, in the presence of oligomycin (1 μg/mL) and/or increasing amounts (2.5–12 μmol/L) of carbonyl cyanide m-chlorophenylhydrazone (CCCP). Leak was calculated in the presence of oligomycin that inhibits ATPase synthase. Maximal respiration was determined with CCCP. The respiration reserve capacity was calculated by subtracting the basal to the maximal respiration. The mitochondrial respiratory control is the basal/leak ratio. Mitochondrial respiration was inhibited by addition of 1 mmol/L potassium cyanide. To measure P/O ratio, ATP production by OXPHOS was evaluated under glutamate-malate conditions with the ATP chemiluminescent assay (Roche) using aliquots of the cell suspension during polarography (20).

Mitochondrial membrane potential

Mitochondrial inner membrane potential was measured as previously described (21) using tetramethylrhodamine ethyl ester perchlorate probe (TMRE).

Respiratory chain spectrophotometric assays

Respiratory chain complex activities were measured on isolated mitochondria resuspended in 300 μL of homogenized buffer (225 mmol/L mannitol, 75 mmol/L saccharose, 10 mmol/L Tris-HCl, 0.1 mmol/L EDTA, pH 7.2) as previously described (22).

Glucose and pyruvate metabolism

Cells in 25 cm^2 flasks were incubated for 3 hours in DMEM containing either 5 mmol/L [U-^{14}C]glucose (0.1 Ci/mole) or no glucose but 6 mmol/L [2-^{14}C]pyruvate (0.1 Ci/mole). Rates of oxidation ($^{14}CO_2$ production) and esterification into phospholipid (^{14}PL), triglyceride (^{14}TG), and diacylglycerol (^{14}DAG) were determined as previously described (23). Pyruvate dehydrogenase activity was measured by the release of $^{14}CO_2$ from

0.1 mmol/L [1-^{14}C]pyruvate. Cells in 25 cm^2 flasks were incubated for 3 hours in no glucose but 0.1 mmol/L [1-^{14}C]pyruvate (1.67 Ci/mole) complemented or not with DCA (10 mmol/L), and $^{14}CO_2$ was determined.

Statistical analysis

Results were expressed as mean ± SEM and analyzed using GraphPad Prism 5 Software. The Mann–Whitney and one-way ANOVA tests were used to compare data sets. Statistical significance was set at $P < 0.05$.

Results

UCP2 overexpression impairs cancer cell proliferation

To investigate the impact of UCP2 on cancer cell proliferation, we used the murine melanoma cell line B16F10, which exhibits a very low endogenous UCP2 expression, to generate two clones stably overexpressing either low (UCP2^{lo}) or high (UCP2^{hi}) level of the full-length mouse UCP2-flag (Fig. 1A). UCP2^{lo} and UCP2^{hi} B16F10 cells respectively showed a 40% and 70% decrease in cell proliferation rate when compared with B16F10 cells (Fig. 1B). In parallel, the potential of B16F10 cells to form *in vitro* colonies was reduced upon UCP2 overexpression by 1.5- and 3-fold in UCP2^{lo} and UCP2^{hi} B16F10, respectively (Fig. 1C). UCP2 impact on cell proliferation was also observed *in vivo*. Immunodeficient mice implanted subcutaneously with B16F10 cells developed bigger tumors than the ones with UCP2^{lo} and UCP2^{hi} B16F10 cells (Fig. 1D). These results highlight the ability of UCP2 to inhibit both tumor cell proliferation and growth.

Modulation of cell proliferation by UCP2 overexpression was also observed in two other human cancer cell lines with low basal UCP2 expression, the pancreatic cancer MIA PaCa-2 and glioblastoma U-87 MG cell lines (Fig. 2A). As observed with B16F10 cells, UCP2 overexpression significantly reduced the potential of tumor cells to form colonies *in vitro* (Fig. 2B). Combined data from the three cell lines showed that cancer cell proliferation was negatively correlated to UCP2 expression ($P < 0.01$, Spearman correlation test; Fig. 2C).

Decreased cell proliferation is associated with cell-cycle dysregulation but not increased apoptosis

The mechanisms underlying the impact of UCP2 on cell proliferation were thereafter addressed in UCP2^{hi} B16F10 cells as compared with B16F10 cells. Expression of p21 protein, a cycling-dependent kinase inhibitor, was strongly upregulated in UCP2^{hi} cells compared with B16F10 cells (Fig. 3A). Cell-cycle analysis revealed in UCP2^{hi} cells a marked reduction of cell number in S-phase (−22.4%) associated with an increased cell number in G_1 phase (+12%; Fig. 3B). The PI3K–Akt (Akt) signaling pathway, known to be constitutively activated through multiple mechanisms in cancer (24), was inhibited in UCP2^{hi} B16F10 cells as shown by the reduced ratio of phospho-Akt (Ser473)/total Akt as well as the decreased phosphorylation of its downstream components p70 S6 Kinase and phospho-s6 ribosomal protein (Fig. 3C). In addition, in basal conditions, the cleaved caspase-3/caspase-3 ratio was not changed in UCP2^{hi} cells compared with B16F10 cells (Fig. 3D), suggesting that UCP2-induced decrease in cell proliferation did not result from increased apoptosis. Decreasing Akt signaling usually represses a powerful prosurvival signaling cascade, which could potently increase the effect of apoptosis-inducing chemotherapeutics, such as staurosporine (STS). STS and its derivatives are protein kinase C inhibitors and prototypical inducers of mitochondria-mediated apoptosis. They have already been used to treat advanced metastatic melanoma in phases I and II of clinical trials (25). To determine whether UCP2 overexpression can amplify apoptosis induced by chemotherapeutic drugs, B16F10 and UCP2^{hi} cells were treated with STS. STS-induced apoptosis was significantly enhanced in UCP2^{hi} cells as shown by the increase in dead cells (+54%; Fig. 3D), caspase-3/7 activities (+64%; Fig. 3E), and cleaved caspase-3/caspase-3 ratio (+45%; Fig. 3F). Moreover, STS-induced death was also significantly enhanced in UCP2^{hi} MIA PaCa-2 and UCP2^{hi} U-87 MG cells as shown by the respective 136% and 60% increase in dead cells (Supplementary Fig. S1A and S1B). Thus, UCP2-induced decrease in cell proliferation was associated with cell-cycle dysregulation and altered cell proliferation signaling.

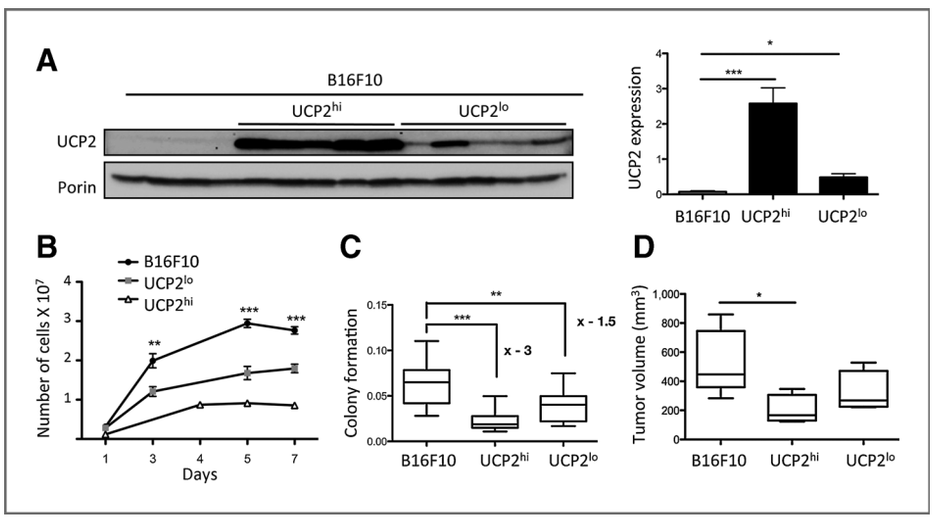

Figure 1. UCP2 expression impairs B16F10 cancer cell proliferation. A, immunoblot analysis of UCP2 protein level in mitochondrial extracts from control (B16F10) cells and B16F10 cells overexpressing high (UCP2^{hi}) or low (UCP2^{lo}) level of UCP2. Porin was used as a loading control for quantification ($n = 5$). B, growth curves from control, UCP2^{hi}, and UCP2^{lo} B16F10 cells. Data, mean ± SEM from three independent cultures. C, colony formation ($n = 5$ independent experiments in triplicate). D, tumor size after xenograft experiments ($n = 7$ for B16F10, $n = 4$ for UCP2^{hi} and UCP2^{lo}). *, $P < 0.05$; **, $P < 0.01$; and ***, $P < 0.001$.

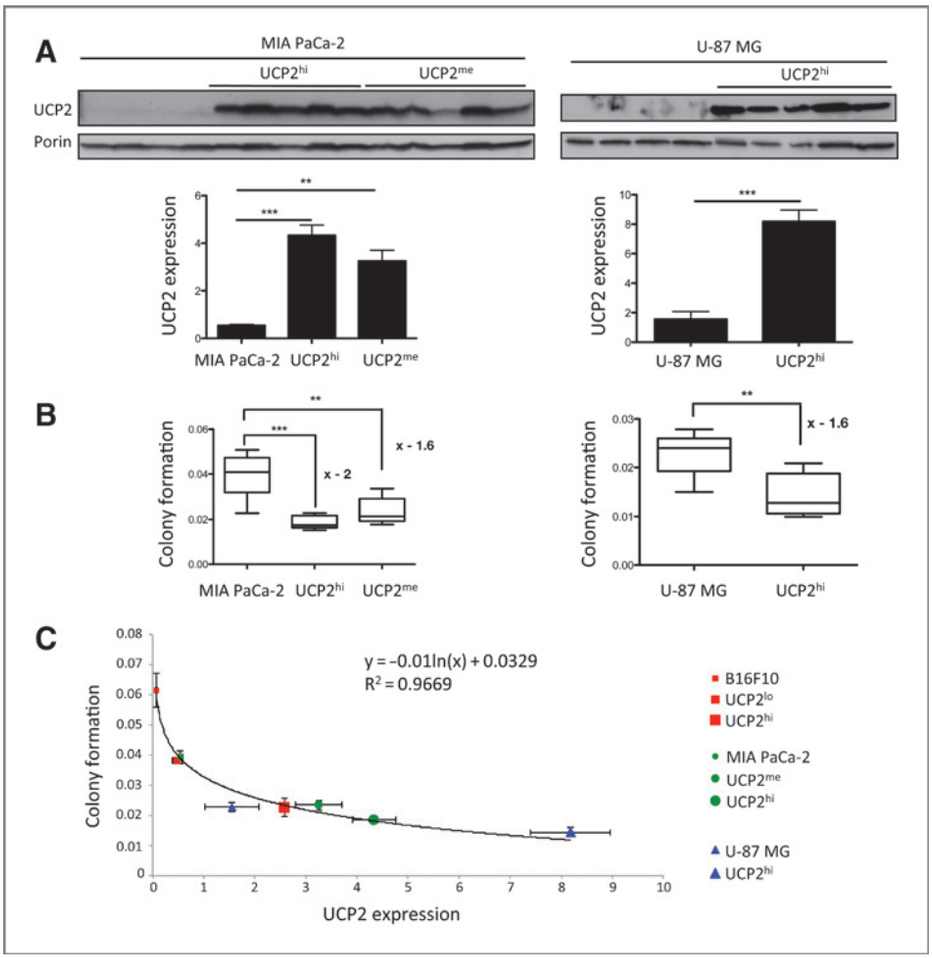

Figure 2. UCP2 expression impairs MIA PaCa-2 and U-87 MG cancer cell proliferation. A, immunoblot analysis of UCP2 protein level in mitochondrial extracts from control MIA PaCa-2 and U-87 MG cells, and clones overexpressing high ($UCP2^{hi}$) or medium ($UCP2^{me}$) level of UCP2. Porin was used as a loading control for quantification ($n = 5$). B, colony formation ($n = 4$ independent experiments in triplicate). C, correlation between UCP2 expression and cancer cell proliferation ($P = 0.004$, Spearman correlation test). **, $P < 0.01$; and ***, $P < 0.001$.

UCP2 increases mitochondrial respiration without uncoupling

We next addressed the metabolic impact of UCP2 overexpression in B16F10 cells. Significant increase in both the basal and maximal oxygen consumption rates was observed together with increased respiration reserve capacity in $UCP2^{hi}$ cells (Fig. 4A). The non–ATP-generating respiration (leak) was increased in parallel, thus maintaining similar respiratory control in the two cell lines (B16F10 cells: 2.70 ± 0.39; $UCP2^{hi}$ cells: 2.35 ± 0.09, $P =$ ns). Mitochondrial membrane potential ($\Delta\psi$) analysis using the fluorescent probe TMRE confirmed that the increased leak had no uncoupling effect. This was true under basal conditions but also in the presence of oligomycin, which induced as expected an increase in $\Delta\psi$, or in the presence of CCCP, which decreased $\Delta\psi$ (Fig. 4B). The lack of uncoupling in $UCP2^{hi}$ cells was further confirmed by their normal P/O ratio (2.35 ± 0.42 *versus* 2.16 ± 0.34 in control cells; $P =$ ns). The increased respiratory capacity in $UCP2^{hi}$ cells did not result from higher mitochondrial content as citrate synthase (CS) protein level and activity were similar to those found in B16F10 cells (Fig. 4C). By contrast, the steady-state amount of several components of the OXPHOS complexes, including subunits of the respiratory complexes I, II, and IV, was significantly increased in mitochondria from $UCP2^{hi}$ cells (Fig. 4D). Spectrophotometric assays of the respiratory complexes activities showed a significant increase in complex IV activity. Complex II activity also increased but without reaching significance (Fig. 4E). UCP2 overexpression thus induces a mitochondrial remodeling with higher OXPHOS expression level per mitochondria, resulting in an enhanced cell respiratory capacity.

Oxidative stress remained unaffected by UCP2 expression

Mitochondrial ROS production, which mainly occurs at complexes I and III, is dependent on the electron flux through the respiratory chain. As UCP2 increased mitochondrial respiration, we investigated whether an increased oxidative stress could be involved in UCP2-induced decrease in cell proliferation. Direct measurement of mitochondrial ROS production (mROS) with the fluorescent probe MitoSox revealed no difference in ROS production between B16F10 and $UCP2^{hi}$ cells in basal conditions or in the presence of inhibitors such as antimycin and oligomycin (Supplementary Fig. S2A). In agreement with these findings, cellular oxidative damages such as protein carbonylation and lipid peroxidation were not increased upon UCP2 overexpression (Supplementary Fig. S2B and S2C). Moreover, the proteasome activity and the amount of the mitochondrial matrix Lon protease, known to be altered by oxidative stress (26), were similar in B16F10 and $UCP2^{hi}$ cells (Supplementary

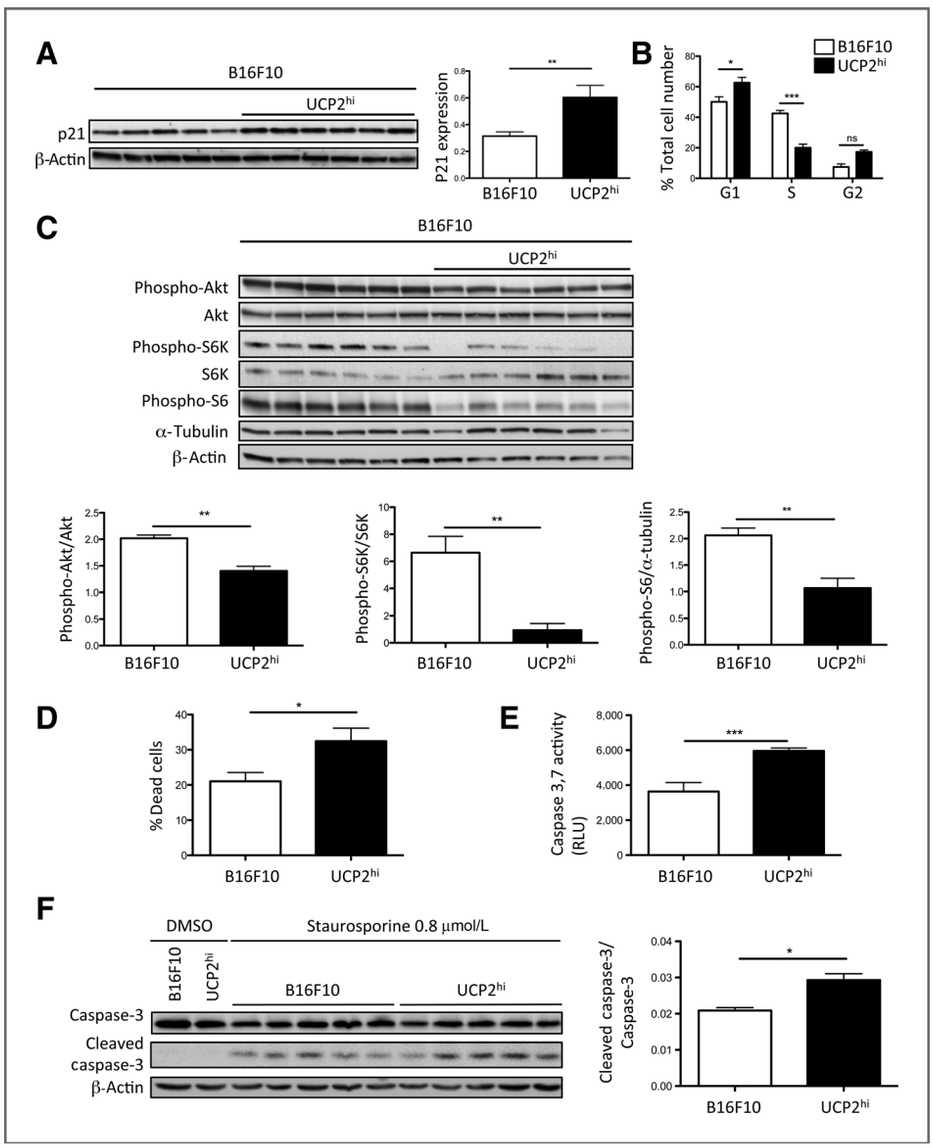

Figure 3. Decreased cell proliferation is associated with cell-cycle dysregulation but not increased apoptosis. A, immunoblot analysis of p21 protein level on whole cell lysates with β-actin as a loading control for quantification ($n = 6$). B, histograms show the percentage of B16F10 and UCP2^{hi} cells in the different cell-cycle phases ($n = 3$). C, immunoblot analysis of phospho-Akt (Ser473), Akt, phospho-S6 Kinase (Thr389), S6 Kinase, and phospho-S6 (Ser240/244) protein levels on whole cell lysates with β-actin and α-tubulin as loading controls for quantification of the phospho-Akt/Akt and phospho-S6K/S6K ratios, and phospho-S6 expression ($n = 6$). D, cells were treated with staurosporine (1 μmol/L) for 6 hours, then stained with Trypan blue. The percentage of dead cells in the whole-cell population ($n = 5$). E, cells were treated for 6 hours with staurosporine (0.8 μmol/L) and caspase-3/7 activities were measured ($n = 5$). F, cells were treated with DMSO or staurosporine (0.8 μmol/L) for 6 hours. Immunoblot analysis of caspase-3 and cleaved caspase-3 protein levels on whole cell lysates with β-actin as a loading control for quantification of the cleaved caspase-3/caspase-3 ratio ($n = 5$). *, $P < 0.05$; **, $P < 0.01$; and ***, $P < 0.001$.

Fig. S2D and S2E). Lastly, the protein expression of ROS detoxification enzymes, such as the cytosolic superoxide dismutase-1 (SOD1) and the mitochondrial SOD2, was not modified (Supplementary Fig. S2F). Finally, treatment with a mitochondria-targeted antioxidant (Mito-TEMPO) did not prevent the decreased proliferation rate of UCP2^{hi} cells (Supplementary Fig. S2G), confirming that mROS was not involved in UCP2-induced decrease in cell proliferation. Taken together, these results indicated that despite an increased mitochondrial respiration, UCP2-overexpressing cells neither have increased ROS production nor oxidative stress.

UCP2 promotes a metabolic reprogramming toward substrate oxidation

In cancer cells, the metabolic shift from oxidative metabolism to elevated aerobic glycolysis (Warburg effect) is in general important for generating precursors for cellular biogenesis to ensure cell proliferation. Therefore, we hypothesized that UCP2 impact on cell proliferation could be based upon metabolism redirection toward oxidation. To address this question, we investigated [U-^{14}C]glucose metabolism by measuring its oxidation into $^{14}CO_2$ as well as the esterification of glucose-derived carbons into diacylglycerol (^{14}DAG), triglyceride (^{14}TG), and phospholipid (^{14}PL; Fig. 5A). No change in the total amount of [U-^{14}C] glucose metabolized was observed (B16F10 cells: 87.1± 3.8 nmol/3h/mg of protein; UCP2^{hi} cells: 86.5 ± 3.6 nmol/3h/mg of protein, P = ns). Interestingly, the metabolic orientation of glucose toward oxidation was significantly increased by UCP2 overexpression (Fig. 5B). In agreement with this result, UCP2^{hi} cells displayed a reduced extracellular acidification rate, which reflected a decrease in lactate production (Fig. 5C). As $^{14}CO_2$ production from [U-^{14}C]glucose depends both on the rate of glycolysis and pyruvate oxidation, we more directly assessed the impact of UCP2 on pyruvate

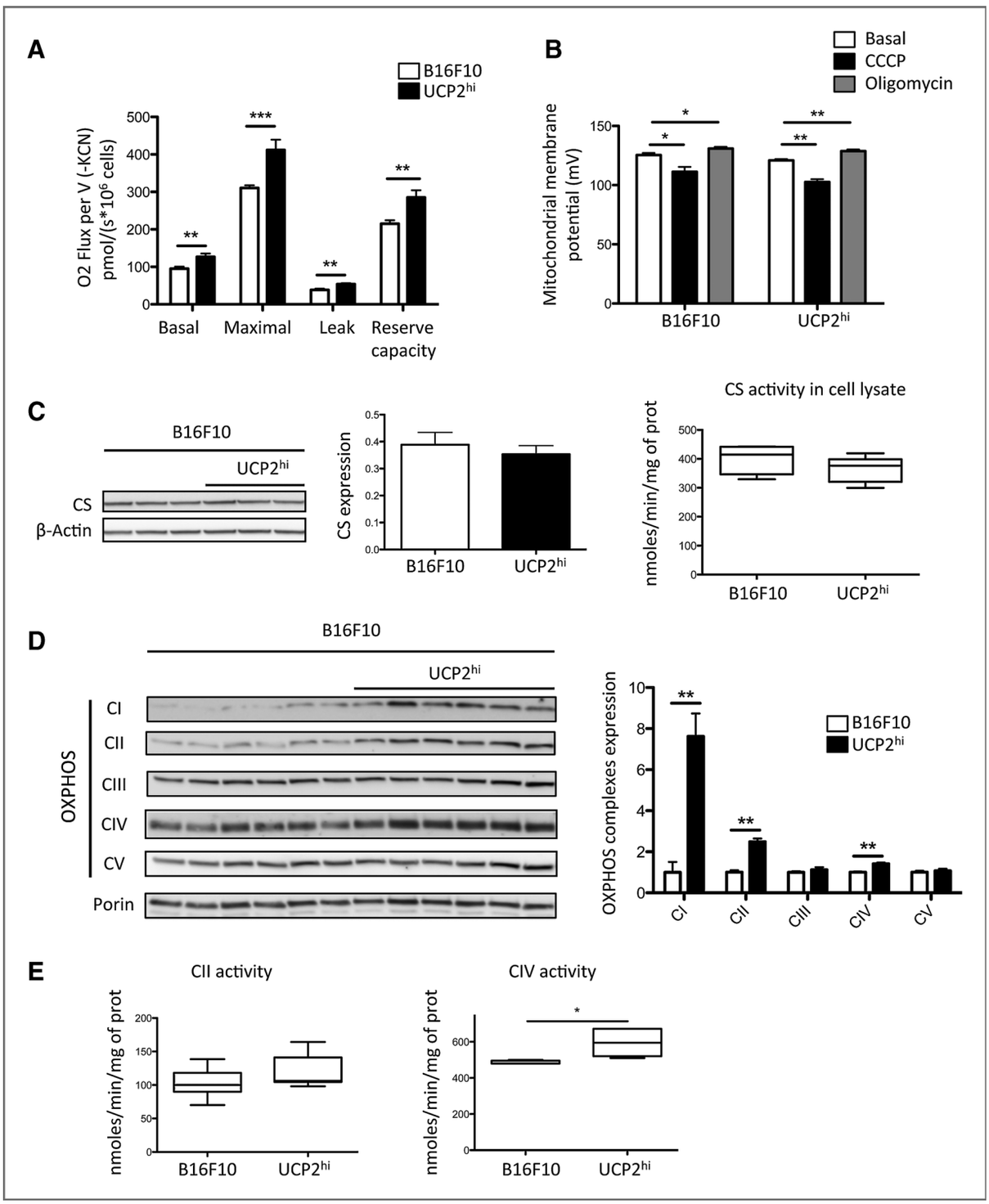

Figure 4. UCP2 increases mitochondrial respiration without uncoupling. A, mitochondrial respiration was determined in basal conditions (DMEM 4 g/L glucose), in the presence of oligomycin (1 μg/mL; leak), and in the presence of increasing amounts of CCCP (1–20 μmol/L) to determine the maximal respiration rate ($n = 10$) and the respiration reserve capacity. B, mitochondrial membrane potential was measured in basal, after depolarization (+ CCCP 2 μmol/L) and hyperpolarization (+ oligomycin 0.5 μg/mL) conditions ($n = 5$). Differences between B16F10 and UCP2^{hi} cells were nonsignificant in all conditions. C, immunoblot analysis of CS protein level on whole cell lysates with β-actin as a loading control. CS activity was measured on whole cell lysates from B16F10 and UCP2^{hi} cells ($n = 5$). D, immunoblot analysis of OXPHOS complexes (CI to CV) protein levels in mitochondrial extracts with porin as a loading control. Quantification of CI, CII, CIII, CIV, and CV expression in UCP2^{hi} cells is expressed relative to control cells ($n = 6$). E, activity of OXPHOS CII ($n = 7$–8) and CIV ($n = 5$) complexes was measured using isolated mitochondria. *, $P < 0.05$; **, $P < 0.01$; and ***, $P < 0.001$.

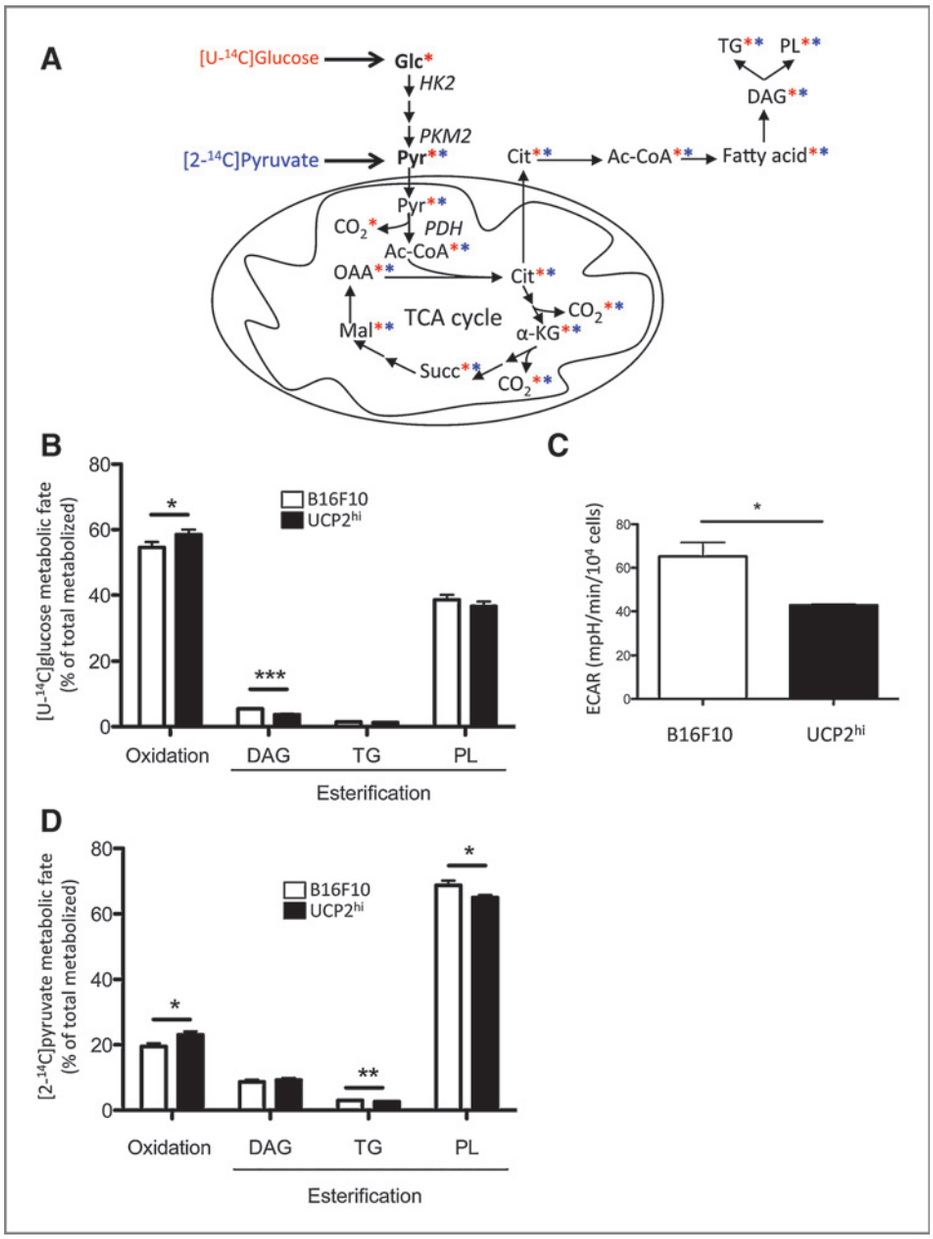

Figure 5. UCP2 promotes a metabolic reprogramming toward substrate oxidation. B16F10 and UCP2^{hi} cells were cultured for 3 hours in the presence of 5 mmol/L [U-^{14}C]Glucose or 6 mmol/L [2-^{14}C]Pyruvate. A, schematic representation of [U-^{14}C]glucose and [2-^{14}C]pyruvate metabolism. *, ^{14}C from glucose (red) and pyruvate (blue). B, [U-^{14}C]glucose metabolic fate toward oxidation ($^{14}CO_2$ production) and esterification into ^{14}DAG, ^{14}TG, and ^{14}PL. Data, percentage of total [U-^{14}C]glucose metabolized (n = 12). C, extracellular acidification rate of B16F10 and UCP2^{hi} cells is an index of lactate production (n = 4). D, [2-^{14}C]pyruvate metabolic fate toward oxidation ($^{14}CO_2$ production) and esterification into ^{14}DAG, ^{14}TG, and ^{14}PL. Data, percentage of total [2-^{14}C]pyruvate metabolized (n = 12). *, $P < 0.05$; **, $P < 0.01$; and ***, $P < 0.001$. Glc, glucose; Pyr, pyruvate; HK2, hexokinase 2; PKM2, pyruvate kinase isoform 2; Ac-CoA, acetyl-CoA; Cit, citrate; α-KG, α-ketoglutarate; Succ, succinate; Mal, malate; OAA, oxaloacetate.

oxidation using [2-^{14}C]pyruvate. Indeed, 2-^{14}C is used to generate $^{14}CO_2$ only during the second round of the TCA cycle and not during pyruvate decarboxylation by the mitochondrial pyruvate dehydrogenase (PDH; Fig. 5A). As for [U-^{14}C]glucose, UCP2 overexpression did not change the total amount of [2-^{14}C]pyruvate metabolized (B16F10 cells: 105.7 ± 6.6 nmol/3h/mg of protein; UCP2^{hi} cells: 116.7 ± 8.8 nmol/3h/mg of protein, P = ns). We observed that both the pyruvate oxidation rate (B16F10 cells: 20.5 ± 1.5 nmol/3h/mg of protein; UCP2^{hi} cells: 27 ± 2.4 nmol/3h/mg of protein, $P < 0.05$) and its metabolic fate toward oxidation (Fig. 5D) were significantly increased in UCP2^{hi} cells compared with B16F10 cells. Conversely, esterification of pyruvate-derived carbons into ^{14}TG and ^{14}PL was specifically decreased in UCP2^{hi} cells (Fig. 5D). These results thus clearly showed that UCP2 overexpression induced a metabolic reprogramming toward pyruvate oxidation.

UCP2-induced metabolic reprogramming involves the HIF/AMPK axis

To further investigate the molecular mechanisms governing UCP2-induced oxidative phenotype, we examined the expression level of two key glycolytic enzymes, hexokinase 2 (HK2) and isoform 2 of pyruvate kinase (PKM2; Fig. 5A). HK2 catalyses the first step of glycolysis, and its mitochondrial localization is known to allow effective reconversion of ATP into ADP (27). UCP2^{hi} cells displayed decreased HK2 expression both at the mRNA (Supplementary Fig. S3A) and protein

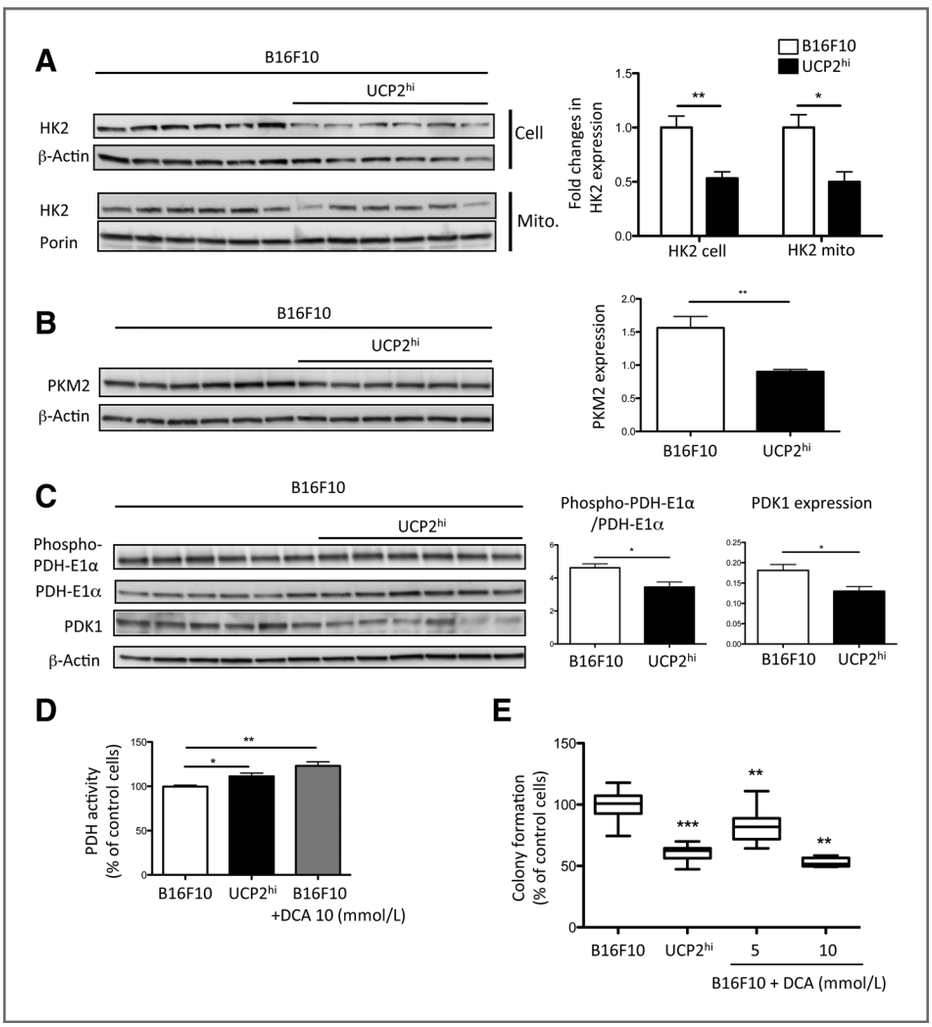

Figure 6. UCP2 increases PDH activity. A, immunoblot analysis HK2 protein level using whole cell lysates and mitochondrial extracts with β-actin and porin as loading controls for quantification, and the values are expressed relative to control cells ($n = 6$). B, immunoblot analysis of PKM2 protein level using whole cell lysates with β-actin as a loading control for quantification. C, immunoblot analysis of pyruvate dehydrogenase (PDH-E1α), phospho-PDH-E1α (Ser293), and PDK1 protein levels using whole cell lysates with β-actin as a loading control for quantification of the phospho-PDH-E1α/PDH-E1α ratio and PDK1 expression ($n = 6$). D, PDH activity was measured by the release of $^{14}CO2$ from 0.1 mmol/L [1-^{14}C]pyruvate in B16F10 cells in the absence or presence of DCA and in UCP2^{hi} cells. Results are expressed as a percentage of control cells ($n = 10$). E, B16F10 and UCP2^{hi} cells were cultured in the absence or presence of DCA, and colony formation was measured ($n = 10$ and 5). Results are expressed as percentage of control cells. *, $P < 0.05$; **, $P < 0.01$; and ***, $P < 0.001$.

(Fig. 6A) levels as well as decreased mitochondrial localization of the protein (Fig. 6A). Pyruvate kinase converts phosphoenolpyruvate into pyruvate. It regulates the proportion of glucose-derived carbons that may be used for energy production. PKM2 isoform is usually overexpressed in tumor cells where its expression is associated with increased glucose uptake and lactate production, but decreased O_2 consumption (28). UCP2^{hi} cells disclosed decreased PKM2 protein expression when compared with B16F10 cells (Fig. 6B).

Once generated by glycolysis, pyruvate is imported into mitochondria through the pyruvate car-rier and converted into acetyl-CoA by PDH. PDH is inactivated through phosphorylation at Ser 293 by PDH kinase 1 (PDK1; refs. 29, 30). The ratio of phospho-PDH-E1/total PDH-E1 was significantly decreased in UCP2^{hi} cells (Fig. 6C), which was associated with a decrease in both PDK1 mRNA (Supplementary Fig. S3B) and protein levels (Fig. 6C), suggesting enhanced PDH activity in UCP2^{hi} cells. Indeed, PDH activity was significantly increased in UCP2^{hi} cells (+12%) compared with B16F10 cells (B16F10 cells: 7.0 ± 0.2 nmol/3h/mg; UCP2^{hi} cells: 7.9 ± 0.2 nmol/3h/mg of protein, $P < 0.05$; Fig. 6D). To determine the importance of PDH regulation in cell proliferation, B16F10 cells were treated with DCA, a PDK1 inhibitor (31), which led to increased PDH activity (+23%; Fig. 6D). DCA treatment disclosed a dose-dependent decrease in B16F10 colony formation, the impact of UCP2 overexpression being within the range effect of DCA (Fig. 6E). These results indicate that UCP2-induced PDH activation is an important mechanism of the UCP2 antitumor action.

HIF1α, one of the main regulators of hypoxia-induced glycolysis, targets several enzymes whose expression was decreased in UCP2^{hi} cells, including PKM2 (32). PKM2 also promotes the Warburg effect by serving as a transcriptional coactivator for HIF1α in cancer cells (33). HIF1α induces PDK1, thus inhibiting PDH (29). HIF1α-dependent metabolic reprogramming of cancer cells is promoted by the disruption of AMPK signaling (34). AMPK senses the cellular energy status through increased AMP/ATP and ADP/ATP ratios (35) and has been linked to tumorigenesis regulation (36). Interestingly, UCP2 overexpression in B16F10 cells led to increased AMPK activity as shown by its increased phosphorylation at Thr172 without change in total AMPK protein expression (Fig. 7A). B16F10 cell treatment with AICAR, an AMPK activator,

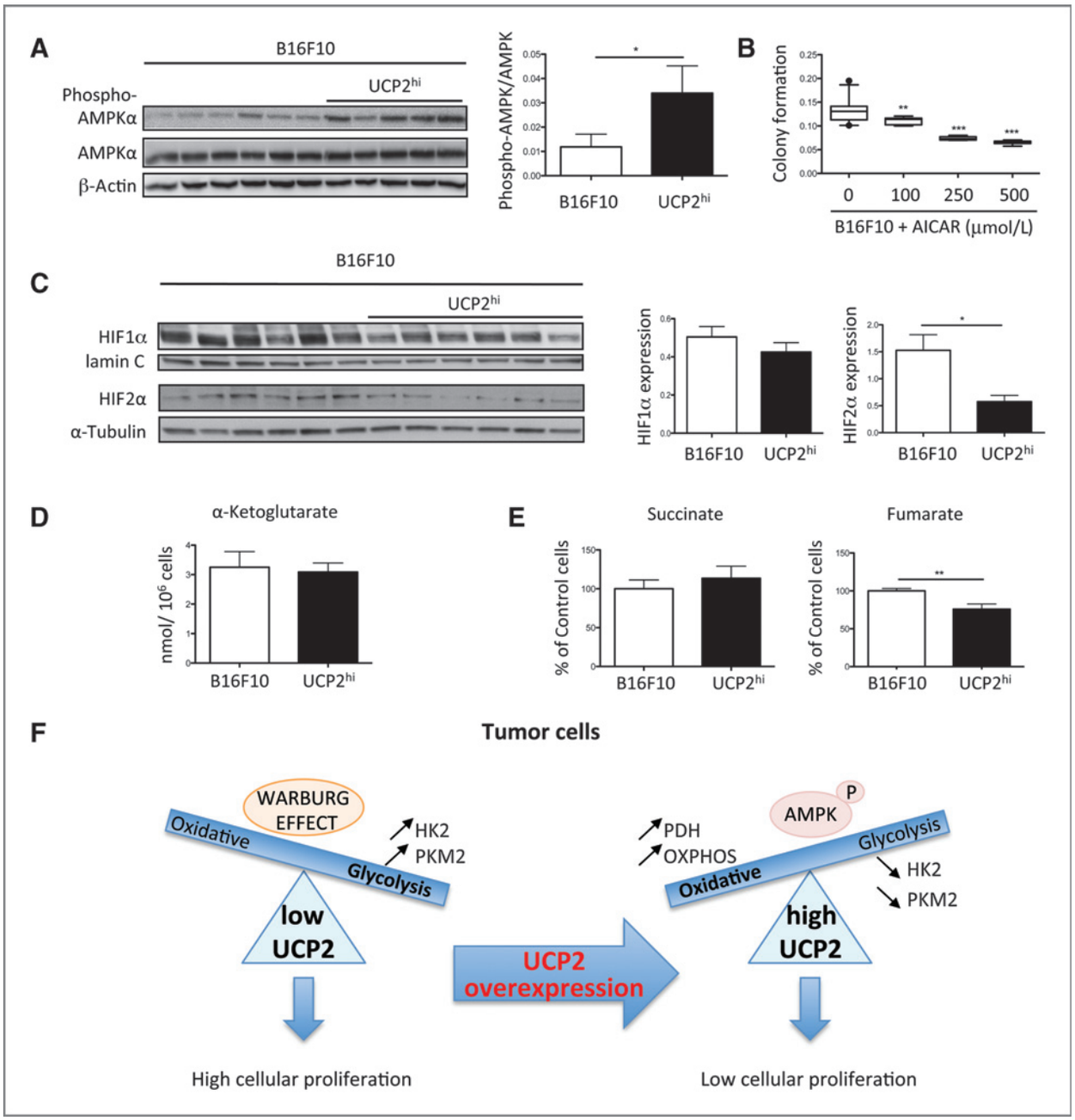

Figure 7. UCP2-induced metabolic reprogramming involves the HIF/AMPK axis. A, immunoblot analysis of phospho-AMPKα (Thr172) and AMPKα protein levels using whole cell lysates with β-actin as a loading control for quantification of the phospho-AMPKα/AMPKα ratio ($n = 6$). B, B16F10 cells were cultured in the presence of 0, 100, 250, or 500 μmol/L AICAR, and colony formation was measured ($n = 10$). C, immunoblot analysis of HIF1α (nuclear lysates) and HIF2α (whole cell lysates) protein levels with lamin A/C (nuclear) and α-tubulin (cellular) as loading controls for quantification ($n = 6$). D, α-Ketoglutarate level in cell extracts was expressed in nmol/10^6 cells ($n = 6$). E, succinate and fumarate levels in cell extracts were expressed as percentage of control cells ($n = 6$). *, $P < 0.05$; **, $P < 0.01$; and ***, $P < 0.001$. F, tumor cells expressing low level of UCP2 present high cellular proliferation rate associated with high expression of HK2 and PKM2 enzymes. UCP2 overexpression in these cells leads to a metabolism reprogramming favoring oxidative metabolism with increased PDH and OXPHOS expression, and conversely decreased HK2 and PKM2 expression. This reprogramming was associated with an increase in AMPK activity.

decreased B16F10 cell proliferation in a dose-dependent manner (Fig. 7B), confirming the involvement of AMPK in B16F10 cell proliferation. Activation of AMPK signaling in UCP2^{hi} cells was associated with a slight decrease in HIF1α and a significant decrease in HIF2α protein expression (Fig. 7C). To investigate the underlying mechanisms, we measured the levels of α-ketoglutarate, succinate, and fumarate, intermediates that participate to the regulation of prolyl hydroxylase

domain (PHD) enzymes responsible for HIF degradation (32). The level of fumarate was significantly decreased by UCP2 overexpression whereas the total amounts of α-ketoglutarate and succinate remained unchanged (Fig. 7D and E).

Discussion

Cancer cells are known to increase their glycolytic activity in the presence of oxygen without a matching increase in their oxidative phosphorylation, a phenomenon known as the Warburg effect (37). Our present study clearly demonstrates that UCP2-induced metabolic reprogramming toward oxidation reduces cancer cell proliferation both *in vitro* and *in vivo*. It therefore provides another demonstration of the tight relationship between metabolism and tumor growth. In the initial hypothesis, the Warburg effect was proposed to be driven through defective mitochondria. Indeed, many cancer cells present mitochondrial alterations such as decreased substrate oxidation, ROS overproduction, mitochondrial DNA mutations, and disturbed control of apoptosis (38). A defective mitochondrial function alters cellular bioenergetics and ultimately reprograms the cell transcription, a process called retrograde signaling (38). Our results show that targeting mitochondrial function through UCP2 can reverse that reprogramming, leading to a return toward lesser glycolysis, higher oxidative phosphorylation capacity and, more importantly, lower cell proliferation rate and tumorigenicity (Fig. 7F).

Actually, UCP2 function itself remains to be fully identified. An uncoupling activity of UCP2 was initially proposed because of UCP2 similarity with UCP1 but still remains controversial (39–43). In the present study, UCP2 overexpression did not uncouple oxidative phosphorylation as shown by the maintained membrane potential, respiratory control, and P/O ratios. It rather modulated mitochondrial substrate routing, likely through transport of metabolites still to be identified. In line with this hypothesis, recent studies have focused on a role of UCP2 in metabolism modulation. Parton and colleagues have shown that UCP2 negatively regulates glucose sensing in neurons and its absence prevents obesity-induced loss of glucose sensing (44). *Ucp2*$^{-/-}$ macrophages had an impaired glutamine metabolism with no evidence, or rather evidence against, an uncoupling role of UCP2 (45). *Ucp2*$^{-/-}$ mouse embryonic fibroblasts exhibited faster proliferative rate associated with decreased mitochondrial fatty acid oxidation and increased glucose metabolism with no evidence for a less-coupled state of mitochondria (18). Therefore, our present study reinforces the role of UCP2 in the regulation of cellular metabolism.

We presently demonstrate that UCP2 overexpression in cancer cells generates a mitochondrial retrograde signaling that modifies expression of glycolytic and oxidative enzymes, leading to enhanced oxidative phosphorylation. We propose that AMPK and HIF link UCP2-induced metabolic shift and reduced cancer cell proliferation and tumorigenicity (Fig. 7F). The observed AMPK activation and decreased HIF expression in UCP2-overexpressing cells were confirmed by the modification of several glycolytic enzymes downstream of HIF. Their impact on cell proliferation was in accordance with the link recently demonstrated between AMPK, HIF1α, and key metabolic checkpoint limiting cell division (34). UCP2-induced AMPK activation was not due to an acute energetic stress because the ATP level remained unchanged and oxidative phosphorylation was increased and well coupled. The role of UCP2 could be explained by the transport of mitochondrial C4 metabolites, as recently proposed (46), such as succinate and fumarate. Interestingly, mutations in SDH and FH genes encoding two enzymes of the TCA cycle, previously associated with cancer (6, 7), led to the mitochondrial accumulation of succinate and fumarate, which inhibits PHD enzymes leading to HIF protein stabilization. UCP2 overexpression was associated with decreased fumarate level that would activate PHD enzymes, and thus decrease HIF protein level. Moreover, it has been reported that phospho-AMPK level was diminished in FH-deficient cells (47). Therefore, the observed decrease in fumarate level in UCP2^{hi} cells provides a link between increased AMPK activity and reduced HIF2α expression.

In our model, UCP2 may function as a metabolic tumor suppressor, limiting the growth of cancer cells by regulating key bioenergetic and biosynthetic pathways required to support cell proliferation (Fig. 7F). Selection against UCP2 may thus represent an important regulatory step in some tumors allowing them to gain a metabolic growth advantage. Reexpression or reactivation of UCP2 may then seem as a winning therapeutic strategy. This may however not apply to every tumor. Indeed, cancer micro-array databases from genome-wide analysis have shown that UCP2 mRNA expression can be either increased or decreased (Supplementary Table S4). UCP2 is essentially controlled in a translational manner (11), it is therefore difficult to consider a correlation between mRNA and protein expression level. Nevertheless, it is noteworthy that tumors derived from normal cells expressing high level of UCP2, such as lymphocytes and colon cells (11), exhibit increased UCP2 mRNA expression (Supplementary Table S4; ref. 48). In leukemia and colon cancer cells, UCP2 overexpression had been reported to have a protumoral effect (49, 50). In contrary, in the other tumors derived from cells with very low basal UCP2 expression, including melanoma, UCP2 mRNA expression is decreased (Supplementary Table S4). We presently showed that in such type of tumors UCP2 overexpression had an antitumoral effect. Therefore, we propose that in these tumors UCP2 expression could be correlated with mitochondrial metabolism and activity, and as such might be a predictive marker in the response of therapeutic treatments targeting tumoral metabolism.

Taken together, our results demonstrate that direct manipulation of mitochondrial activity by expression of the membrane transporter UCP2 induces a feed-forward loop from mitochondria to the AMPK/HIF axis that modifies the transformed phenotype of cancer cells. This sets up UCP2 as a critical regulator of cellular metabolism with a relevant action against tumor maintenance and malignancy.

Disclosure of Potential Conflicts of Interest

No potential conflicts of interest were disclosed.

Authors' Contributions

Conception and design: A. Lombès, M.-C. Alves-Guerra
Development of methodology: F. Bouillaud, A.-L. Bulteau, A. Lombès, C. Prip-Buus, M.-C. Alves-Guerra
Acquisition of data (provided animals, acquired and managed patients, provided facilities, etc.): P. Esteves, C. Ransy, C. Esnous, V. Lenoir, A. Lombès, M.-C. Alves-Guerra
Analysis and interpretation of data (e.g., statistical analysis, biostatistics, computational analysis): P. Esteves, C. Prip-Buus, M.-C. Alves-Guerra
Writing, review, and or revision of the manuscript: P. Esteves, C. Pecqueur, F. Bouillaud, A. Lombès, C. Prip-Buus, D. Ricquier, M.-C. Alves-Guerra
Administrative, technical, or material support (i.e., reporting or organizing data, constructing databases): F. Bouillaud, M.-C. Alves-Guerra
Study supervision: M.-C. Alves-Guerra

Acknowledgments

The authors thank Céline Bouquet (BioAlliance Pharma) for providing kindly B16F10, MIA PaCa-2, and U-87 MG cells. They also thank Dr. C. Ottolenghi for the mass spectrometry analysis (Reference Center of Inherited Metabolic Diseases, University Paris Descartes, Hospital Necker Enfants Malades, APHP, Paris, France).

Grant Support

This work was financially supported by grants from the "Centre National de la Recherche Scientifique" (CNRS), by the "Institut National de la Santé et de la Recherche Médicale" (INSERM), the University Paris Descartes, and the Ministère de la Recherche.

The costs of publication of this article were defrayed in part by the payment of page charges. This article must therefore be hereby marked *advertisement* in accordance with 18 U.S.C. Section 1734 solely to indicate this fact.

Received December 2, 2013; revised April 1, 2014; accepted April 21, 2014; published OnlineFirst May 22, 2014.

References

1. Hanahan D, Weinberg RA. Hallmarks of cancer: the next generation. Cell 2011;144:646–74.
2. DeBerardinis RJ, Lum JJ, Hatzivassiliou G, Thompson CB. The biology of cancer: metabolic reprogramming fuels cell growth and proliferation. Cell Metab 2008;7:11–20.
3. Wellen KE, Thompson CB. Cellular metabolic stress: considering how cells respond to nutrient excess. Mol Cell 2010;40:323–32.
4. Jones RG, Thompson CB. Tumor suppressors and cell metabolism: a recipe for cancer growth. Genes Dev 2009;23:537–48.
5. Gogvadze V, Orrenius S, Zhivotovsky B. Mitochondria in cancer cells: what is so special about them? Trends Cell Biol 2008;18:165–73.
6. Tomlinson IP, Alam NA, Rowan AJ, Barclay E, Jaeger EE, Kelsell D, et al. Germline mutations in FH predispose to dominantly inherited uterine fibroids, skin leiomyomata and papillary renal cell cancer. Nat Genet 2002;30:406–10.
7. Pollard PJ, Wortham NC, Tomlinson IP. The TCA cycle and tumorigenesis: the examples of fumarate hydratase and succinate dehydrogenase. Ann Med 2003;35:632–9.
8. Yan H, Parsons DW, Jin G, McLendon R, Rasheed BA, Yuan W, et al. IDH1 and IDH2 mutations in gliomas. N Engl J Med 2009;360:765–73.
9. Kroemer G, Pouyssegur J. Tumor cell metabolism: cancer's Achilles' heel. Cancer Cell 2008;13:472–82.
10. Fleury C, Neverova M, Collins S, Raimbault S, Champigny O, Levi-Meyrueis C, et al. Uncoupling protein-2: a novel gene linked to obesity and hyperinsulinemia. Nat Genet 1997;15:269–72.
11. Pecqueur C, Alves-Guerra MC, Gelly C, Levi-Meyrueis C, Couplan E, Collins S, et al. Uncoupling protein 2, in vivo distribution, induction upon oxidative stress, and evidence for translational regulation. J Biol Chem 2001;276:8705–12.
12. Hurtaud C, Gelly C, Bouillaud F, Levi-Meyrueis C. Translation control of UCP2 synthesis by the upstream open reading frame. Cell Mol Life Sci 2006;63:1780–9.
13. Rousset S, Mozo J, Dujardin G, Emre Y, Masscheleyn S, Ricquier D, et al. UCP2 is a mitochondrial transporter with an unusual very short half-life. FEBS Lett 2007;581:479–82.
14. Arsenijevic D, Onuma H, Pecqueur C, Raimbault S, Manning BS, Miroux B, et al. Disruption of the uncoupling protein-2 gene in mice reveals a role in immunity and reactive oxygen species production. Nat Genet 2000;26:435–9.
15. Blanc J, Alves-Guerra MC, Esposito B, Rousset S, Gourdy P, Ricquier D, et al. Protective role of uncoupling protein 2 in atherosclerosis. Circulation 2003;107:388–90.
16. Alves-Guerra MC, Rousset S, Pecqueur C, Mallat Z, Blanc J, Tedgui A, et al. Bone marrow transplantation reveals the in vivo expression of the mitochondrial uncoupling protein 2 in immune and nonimmune cells during inflammation. J Biol Chem 2003;278:42307–12.
17. Vogler S, Pahnke J, Rousset S, Ricquier D, Moch H, Miroux B, et al. Uncoupling protein 2 has protective function during experimental autoimmune encephalomyelitis. Am J Pathol 2006;168:1570–5.
18. Pecqueur C, Bui T, Gelly C, Hauchard J, Barbot C, Bouillaud F, et al. Uncoupling protein-2 controls proliferation by promoting fatty acid oxidation and limiting glycolysis-derived pyruvate utilization. FASEB J 2008;22:9–18.
19. Ahmed EK, Rogowska-Wrzesinska A, Roepstorff P, Bulteau AL, Friguet B. Protein modification and replicative senescence of WI-38 human embryonic fibroblasts. Aging Cell 2010;9:252–72.
20. Aure K, Mamchaoui K, Frachon P, Butler-Browne GS, Lombes A, Mouly V. Impact on oxidative phosphorylation of immortalization with the telomerase gene. Neuromuscul Disord 2007;17:368–75.
21. Stavru F, Bouillaud F, Sartori A, Ricquier D, Cossart P. Listeria monocytogenes transiently alters mitochondrial dynamics during infection. Proc Natl Acad Sci U S A 2011;108:3612–7.
22. Medja F, Allouche S, Frachon P, Jardel C, Malgat M, Mousson de Camaret B, et al. Development and implementation of standardized respiratory chain spectrophotometric assays for clinical diagnosis. Mitochondrion 2009;9:331–9.
23. Akkaoui M, Cohen I, Esnous C, Lenoir V, Sournac M, Girard J, et al. Modulation of the hepatic malonyl-CoA-carnitine palmitoyltransferase 1A partnership creates a metabolic switch allowing oxidation of de novo fatty acids. Biochem J 2009;420:429–38.
24. Engelman JA. Targeting PI3K signalling in cancer: opportunities, challenges and limitations. Nat Rev Cancer 2009;9:550–62.
25. Kortmansky J, Shah MA, Kaubisch A, Weyerbacher A, Yi S, Tong W, et al. Phase I trial of the cyclin-dependent kinase inhibitor and protein kinase C inhibitor 7-hydroxystaurosporine in combination with Fluorouracil in patients with advanced solid tumors. J Clin Oncol 2005;23:1875–84.
26. Bota DA, Van Remmen H, Davies KJ. Modulation of Lon protease activity and aconitase turnover during aging and oxidative stress. FEBS Lett 2002;532:103–6.
27. Arora KK, Pedersen PL. Functional significance of mitochondrial bound hexokinase in tumor cell metabolism. Evidence for preferential phosphorylation of glucose by intramitochondrially generated ATP. J Biol Chem 1988;263:17422–8.
28. Christofk HR, Vander Heiden MG, Harris MH, Ramanathan A, Gerszten RE, Wei R, et al. The M2 splice isoform of pyruvate kinase is important for cancer metabolism and tumour growth. Nature 2008;452:230–3.
29. Kim JW, Tchernyshyov I, Semenza GL, Dang CV. HIF-1-mediated expression of pyruvate dehydrogenase kinase: a metabolic switch required for cellular adaptation to hypoxia. Cell Metab 2006;3:177–85.
30. Papandreou I, Cairns RA, Fontana L, Lim AL, Denko NC. HIF-1 mediates adaptation to hypoxia by actively downregulating mitochondrial oxygen consumption. Cell Metab 2006;3:187–97.
31. Kato M, Li J, Chuang JL, Chuang DT. Distinct structural mechanisms for inhibition of pyruvate dehydrogenase kinase isoforms by AZD7545, dichloroacetate, and radicicol. Structure 2007;15:992–1004.

32. Denko NC. Hypoxia, HIF1 and glucose metabolism in the solid tumour. Nat Rev Cancer 2008;8:705–13.
33. Luo W, Hu H, Chang R, Zhong J, Knabel M, O'Meally R, et al. Pyruvate kinase M2 is a PHD3-stimulated coactivator for hypoxia-inducible factor 1. Cell 2011;145:732–44.
34. Faubert B, Boily G, Izreig S, Griss T, Samborska B, Dong Z, et al. AMPK is a negative regulator of the Warburg effect and suppresses tumor growth in vivo. Cell Metab 2013;17:113–24.
35. Hardie DG. AMP-activated/SNF1 protein kinases: conserved guardians of cellular energy. Nat Rev Mol Cell Biol 2007;8:774–85.
36. Shackelford DB, Shaw RJ. The LKB1-AMPK pathway: metabolism and growth control in tumour suppression. Nat Rev Cancer 2009;9:563–75.
37. Warburg O. On respiratory impairment in cancer cells. Science 1956;124:269–70.
38. Wallace DC. Mitochondria and cancer. Nat Rev Cancer 2012;12:685–98.
39. Rial E, Gonzalez-Barroso M, Fleury C, Iturrizaga S, Sanchis D, Jimenez-Jimenez J, et al. Retinoids activate proton transport by the uncoupling proteins UCP1 and UCP2. EMBO J 1999;18:5827–33.
40. Jaburek M, Miyamoto S, Di Mascio P, Garlid KD, Jezek P. Hydroperoxy fatty acid cycling mediated by mitochondrial uncoupling protein UCP2. J Biol Chem 2004;279:53097–102.
41. Echtay KS, Winkler E, Frischmuth K, Klingenberg M. Uncoupling proteins 2 and 3 are highly active H(+) transporters and highly nucleotide sensitive when activated by coenzyme Q (ubiquinone). Proc Natl Acad Sci U S A 2001;98:1416–21.
42. Echtay KS, Roussel D, St-Pierre J, Jekabsons MB, Cadenas S, Stuart JA, et al. Superoxide activates mitochondrial uncoupling proteins. Nature 2002;415:96–9.
43. Couplan E, del Mar Gonzalez-Barroso M, Alves-Guerra MC, Ricquier D, Goubern M, Bouillaud F. No evidence for a basal, retinoic, or superoxide-induced uncoupling activity of the uncoupling protein 2 present in spleen or lung mitochondria. J Biol Chem 2002;277:26268–75.
44. Parton LE, Ye CP, Coppari R, Enriori PJ, Choi B, Zhang CY, et al. Glucose sensing by POMC neurons regulates glucose homeostasis and is impaired in obesity. Nature 2007;449:228–32.
45. Nubel T, Emre Y, Rabier D, Chadefaux B, Ricquier D, Bouillaud F. Modified glutamine catabolism in macrophages of Ucp2 knock-out mice. Biochim Biophys Acta 2008;1777:48–54.
46. Vozza A, Parisi G, De Leonardis F, Lasorsa FM, Castegna A, Amorese D, et al. UCP2 transports C4 metabolites out of mitochondria, regulating glucose and glutamine oxidation. Proc Natl Acad Sci U S A 2014;111:960–5.
47. Tong WH, Sourbier C, Kovtunovych G, Jeong SY, Vira M, Ghosh M, et al. The glycolytic shift in fumarate-hydratase-deficient kidney cancer lowers AMPK levels, increases anabolic propensities and lowers cellular iron levels. Cancer Cell 2011;20:315–27.
48. Horimoto M, Resnick MB, Konkin TA, Routhier J, Wands JR, Baffy G. Expression of uncoupling protein-2 in human colon cancer. Clin Cancer Res 2004;10:6203–7.
49. Samudio I, Fiegl M, McQueen T, Clise-Dwyer K, Andreeff M. The Warburg effect in leukemia-stroma cocultures is mediated by mitochondrial uncoupling associated with uncoupling protein 2 activation. Cancer Res 2008;68:5198–205.
50. Derdak Z, Mark NM, Beldi G, Robson SC, Wands JR, Baffy G. The mitochondrial uncoupling protein-2 promotes chemoresistance in cancer cells. Cancer Res 2008;68:2813–9.